VI International Conference on Computational Bioengineering
ICCB 2015
M. Cerrolaza and S.Oller (Eds)

COMPUTATIONAL FLUID DYNAMICS OF A PEDIATRIC VENTRICULAR ASSIST DEVICE

ICCB 2015

JOÃO A. ISLER*, BRUNO S. CARMO*, JULIO R. MENEGHINI*AND IDÁGENE A. CESTARI †

* Department of Mechanical Engineering, Escola Politécnica, University of São Paulo
Av. Prof. Melo Morais, 2231, Cidade Universitária, São Paulo 05508-030, SP, Brazil
E-mail: joao.isler@usp.br

† Heart Institute (InCor), University of São Paulo Medical School, Bioengineering Division
Av. Dr. Eneas de Carvalho Aguiar, 44/SS, Cerqueira Cesar, São Paulo 05403-000, SP, Brasil

Key words: Pediatric ventricular assist device, Artificial heart, Computational fluid mechanics

Abstract. A computational fluid dynamics model is developed to assess the performance of a 35 cc pediatric ventricular assist device. In order to improve the hydrodynamics performance of the device and proposing changes in its design. Computational analyses was carried out for steady and pulsatile flows. Flow patterns, velocity fields and wall shear stresses were analyzed to evaluate the performance of the device.

1 INTRODUCTION

Ventricular assist devices (VADs) are mechanical circulatory support systems for treatment of end-stage heart failure. They can be used as a heart transplant, bridge to recovery or destination therapy [1,2]. These devices have been applied for temporary and long-term support, being used as a continuous support in adults for more than five years [1]. These characteristics are extremely important for patients awaiting heart transplantation, especially in case of small children, because of the difficulty of finding a compatible donor [1]. However, patients who use VAD still suffer from an unacceptable rate of survival, although the treatment with VAD has obtained better results compared to medicines [3]. Despite the extensive acceptance of VADs in adults, their use in small children and infants still bring problems caused by the low frequency pumping that should be used to ensure adequate blood flow, which restults in high thromboembolic risk [4,5].

Pediatric ventricular assist devices (PVADs) are confectioned with geometry and materials similar to those employed in adults versions, but in general, present higher rate of hemolysis and thrombus formation, which remains an obstacle to the development of these devices. The difference in their geometries, such as smaller volume and diameter of the orifices of the valves provide lower blood flow in PVADs. These factors influence the flow features, because they generate turbulence and high shear stress during long periods of pumping cycle, causing hemolysis or pre-rupture of the red blood cells [6]. At the same time, substances released from the red cells during hemolysis influence platelet activation, which combined with regions of

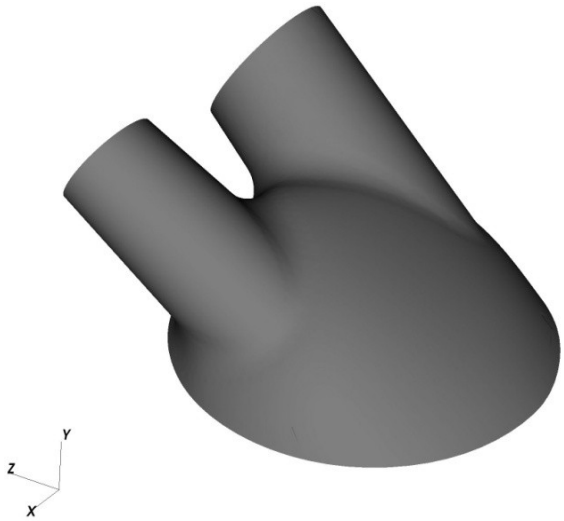

Figure 1: The 35 cc PVAD geometry.

stagnant flow or low shear stresses in the vicinity of the solid walls cause thrombus formation [7].

In order to avoid such complication in the treatment of small children a 35 cc PVAD have been under development in the Heart Institute of the Clinical Hospital of São Paulo (InCor), destined to patients under 25 kg of body weight. Thus, to achieve this goal, a computational model has been developing to better understanding of the flow field within of the device, and its relation to thrombus formation and the occurrence of hemolysis, which are the greatest obstacles to its development.

The aim of this work is to show the first computational simulations of the pneumatic InCor PVAD under development, discuss the flow features within the device and assess regions of high and low wall shear stresses (WSS) and flow stagnation, which are critical areas of blood cell lysis, platelet activation and thrombus formation.

2 METHODS

2.1 Model Geometry

The 35 cc InCor PVAD under development is a pulsatile device for paracorporeal use, and it is confectioned making use of the same materials and principles of operation of a VAD developed for adults. The pulsatile pump is a disposable ventricular prosthesis, with biocompatible material. This pump comprises two chambers: pneumatic and sanguine, separated by a medical grade polyurethane flexible diaphragm to act as a blood contacting surface. The blood chamber has one input and one output, in which connectors for cannulas and bovine pericardial valves prostheses are accommodated (22 mm mitral and 14 mm aortic), ensuring a unidirectional flow through the device. However, for all simulations carried out in this work, the mitral and aortic valves were removed, so that there is no obstruction to the flow get inside the device. In addition, the flexible membrane which separates pneumatic and sanguine chamber is fixed (Figure 1).

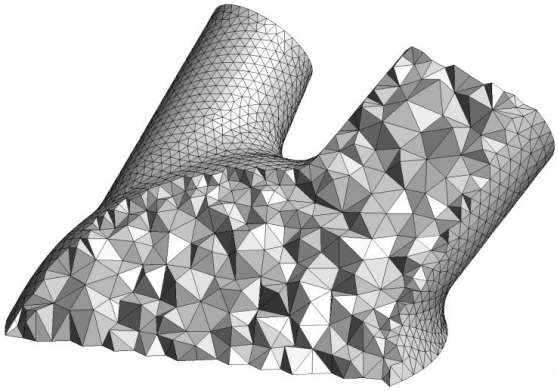

Figure 2: Computational mesh used for both steady and pulsatile flows.

2.2 Computational simulations

An unsteady three-dimensional computational fluid dynamics (CFD) model was developed to assess the performance of the 35 cc pneumatic PVAD in steady and pulsatile flows. In this study, blood was treated as a incompressible Newtonian fluid. Numerical simulations were carried out using the Spectral/*hp* Element Method [8], which is a high-order method. This method has a very low numerical error, high geometric flexibility and it has been successfully used in modeling of biological flows [9,10]. For the cases investigates in this work, blood is governed by the Navier-Stokes equations.

2.3 Grid generation

The Spectral/*hp* element method was applied to simulate blood flow inside the device, which require that the computational domain needs to be subdivided into elements. The total number of volume elements constructed for the PVAD was 28663 tetrahedral elements, the mesh is shown in figure 2. This mesh was used for both computational simulations with steady and pulsatile flows. Since high-order polynomials can represent the solution within each element of the mesh, the mesh generated in this study was made relatively coarse. In the steady case, we used a sixth order polynomial, which corresponds in terms of degrees of freedom, to meshes of approximately 10^7 tetrahedral elements. For pulsatile flow, we employed a seventh order polynomial, which results in approximately 1.4×10^7 degrees of freedom. The triangular external faces of the tetrahedral elements were curved using SPHERIGON patches [11], following a method developed by Plata [12]. Therefore, although the mesh has elements with large size the surface mesh is curvilinear.

2.4 Modeling parameters and boundary condition

As blood is a viscous incompressible fluid, we can define the Reynolds number (*Re)* $\rho u_o D_o / \mu$ with ρ the blood density, μ the blood dynamic viscosity, u_o the inflow velocity and D_o the diameter of the mitral port. Assuming the $\rho = 1044$ kg/m^3 [10], $\mu = 4.043 \times 10^{-3}$ kg/ms [10] and $D_o = 22$ mm. In the steady flow analysis, we applied a spatially uniform velocity profile at the inlet port (mitral), with velocity of $u_o = 0.20$ m/s. This results in a Reynolds number of *Re* = 1136 . For the time-dependent flow dynamics, the velocity wave-

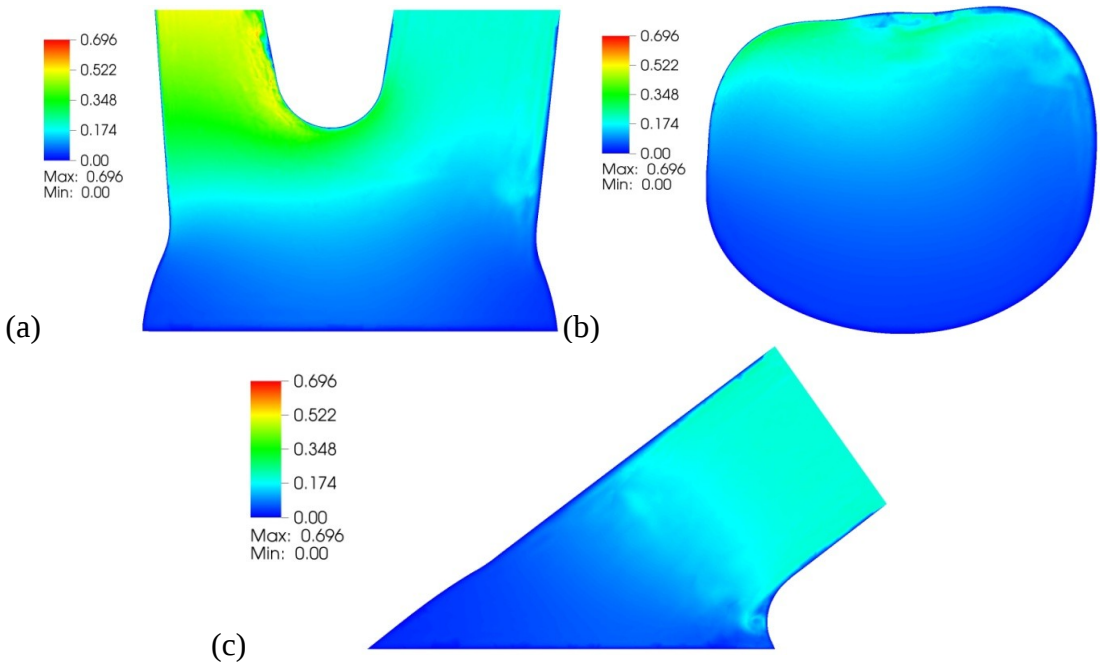

Figure 3: Contours of magnitude velocity (m/s) for the steady flow for slices corresponding to (a) 35 degrees from the plane xz, (b) 6.5 mm from the back face (plane xz), (c) 8 degrees from the plane yz.

form applied was a single-harmonic pulse, given by

$$u(t) = u_m\left[1+\sin\left(2\pi t/T\right)\right], \tag{1}$$

where u_m is the mean velocity, with $u_m = 15$ m/s. The Reynolds number for the pulsatile flow was based on the mean inlet velocity, thus *Re* = 852. In both steady and pulsatile cases, the pressure and the velocity gradient was set up to zero at the outlet boundary condition. A no-slip condition was imposed at the device walls.

3 RESULTS

3.1 Steady flow

Figure 3, shows the contours of magnitude velocity for the steady flow in three different slices. Three important observations can be made. Firstly, there is separated flow in the right wall of the outflow (Figure 3(a)), and it has velocity slightly higher and non-uniform in this region, indicating that the flow may be turbulent. Secondly, the flow does not penetrate too deep in the device, because of the low velocity at the base of the device. Finally, in figure 3(c), we can see the formation of a vortex at the base of the device, which can eventually promote lysis of the red blood cells.

Streamlines of blood flow inside the device are shown in figure 4 for the steady flow. In figure 4(a), we can easily see that there is only few streamlines which establish a good rotational pattern near the border walls of the device. Most of the streamlines go straight away to the outflow without “washing” the device. Figure 4(b), illustrates a unusual pattern formed by the streamlines. The streamlines from the inflow establish a spiral pattern at the base of the

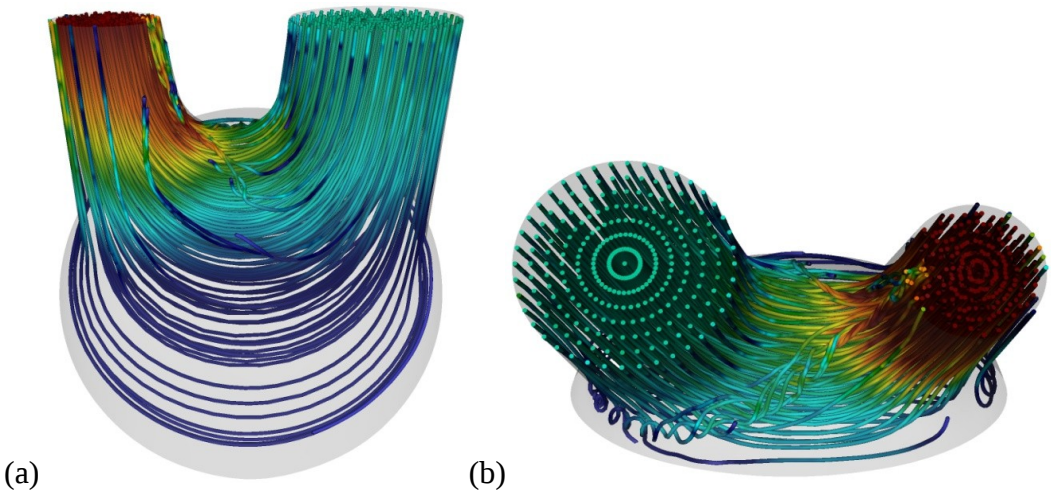

(a) (b)

Figure 4: Streamlines of blood flow in the PVAD for the steady flow. (a) Top view, (b) Side view.

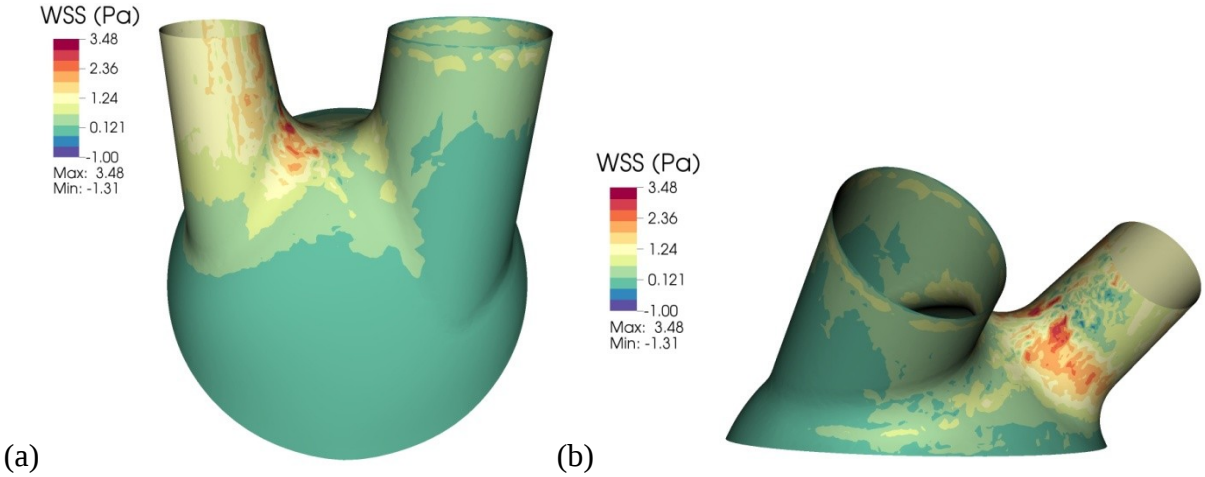

(a) (b)

Figure 5: Colour maps of WSS (Pa) in the PVAD for the steady flow. (a) Top view, (b) Side view

device, which corresponds to the vortex formation in the figure 3(c). Afterwads the spiral pattern goes through the outflow where it joins with another one formed at the top of the device. Flow stagnantion is also observed at the bottom of the outflow region, which could be a critical area of thombus deposition.

Figure 5, shows colour maps of WSS within the device for the steady flow. In figure 5(a), a low WSS is found at the top wall and in the right side of the inflow region of the device. This occurs due to the low velocity observed in these regions, as mentioned before. Although most part of the device has low WSS, a relatively high WSS is observed near the entrance of the outflow region followed by a region with the lowest WSS (Figure 5(b)). This is explained by the separation of the flow in this region associated with the highest velocities in the device. Hubbed and McIntire [13] reported that a wall shear rate (WSR) below than 500 s^{-1} [18 dynes/cm² for a viscosity of 3.5 centipoise] could afford clot formation and deposition on the

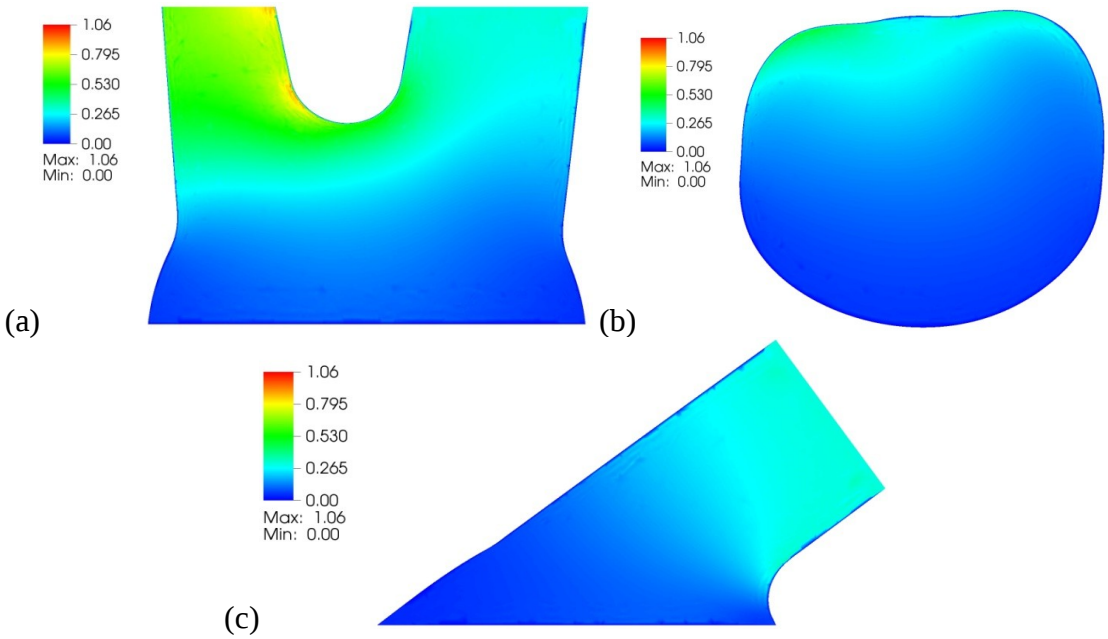

Figure 6: Contours of magnitude velocity (m/s) for the pulsatile flow slices corresponding to (a) 35 degrees from the plane xz, (b) 6.5 mm from the back face (plane xz), (c) 8 degrees from the plane yz.

segmented polyurethane. Therefore, as most part of the device the WSR is below than 500 s^{-1}, attention should be given to the regions with low WSS in the device, in order to improve its performance. However, the diaphragm and valves were removed in this model, consequently the velocities in the inflow and chamber tend to be lower. Normally, the valves impose strong inflow jets which establish a better rotational "washing" pattern, in addition there is no pump to push the fluid out of the device. Thus, the PVAD with these two components will significantly increase the WSS in the device walls. It should be noted as well, that a WSR above than 500 s^{-1} the blood behave as Newtonian fluid [14], then a non-Newtonian fluid need to be employed to better represent flow field within the PVAD.

3.2 Pulsatile flow

For the analyses done in this section, we used figures in the instant of time for which the velocity in the inflow is the highest. In figure 6, we illustrate the contours of magnitude velocity for the pulsatile flow in three different slices. The flow field at this instant of time is very similar to the steady case, with slight differences. We can see, in figure 6(a), that although the velocity is higher than in the steady case, the separated flow in the outflow region is smoother. As previously, the flow does not penetrate too deep in the device and low velocity is found at the base of the device. Nevertheless, there is not vortex formation at the base of the device, close to the inflow region (Figure 6(c)).

Streamlines of blood flow inside the device are shown in figure 7 for the pulsatile flow. The streamlines do not establish a rotational "washing" pattern in the device like in the steady case, with most of the streamlines taking the outflow path (Figure 7(a)). In addition, there are two points of stagnation flow, both being at the base of the device. The first one is close to the inflow region and the second one is close to the outflow region, being potential areas of clot

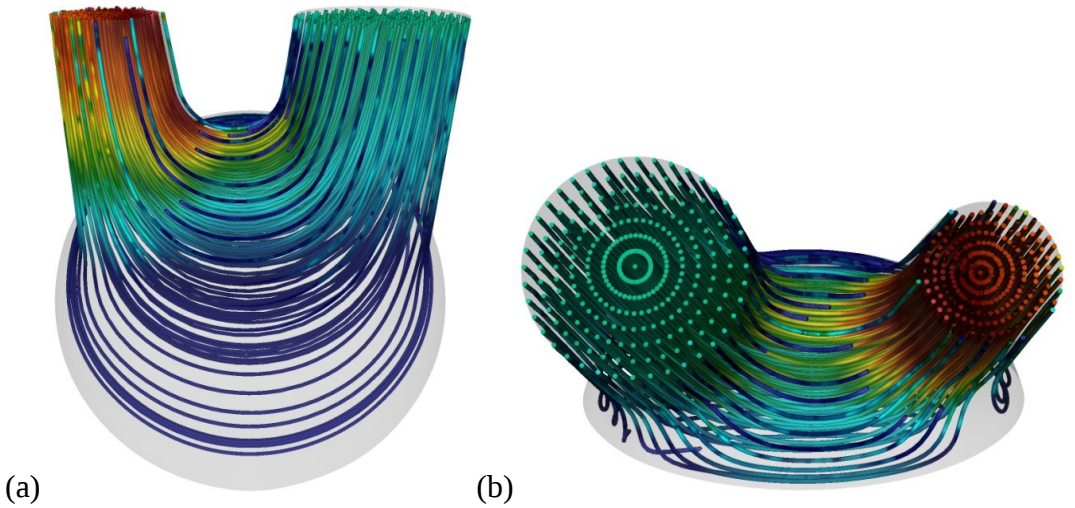

(a) (b)

Figure 7: Streamlines of blood flow in the PVAD for the pulsatile flow. (a) Top view, (b) Side view.

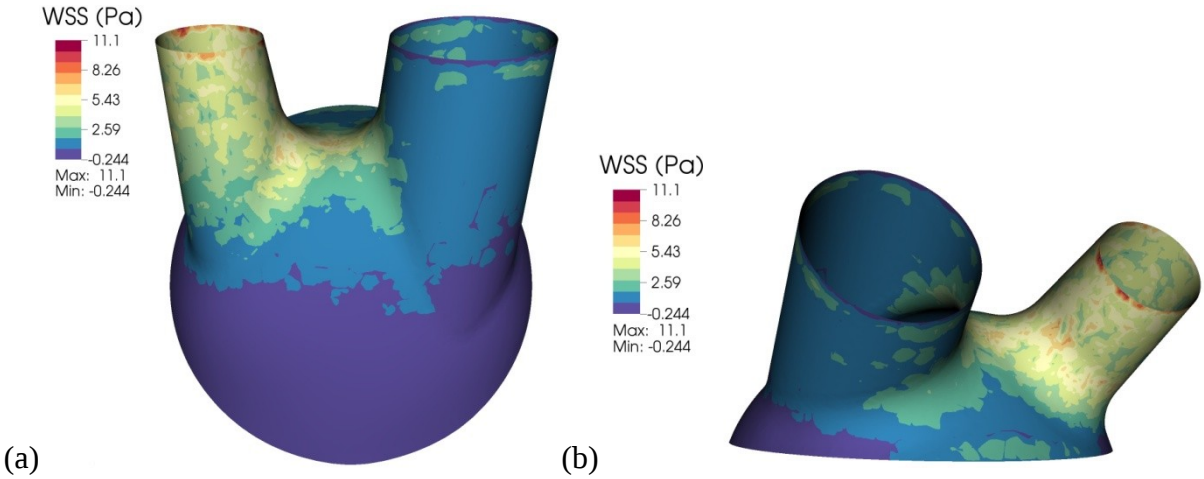

(a) (b)

Figure 8: Colour maps of WSS (Pa) in the PVAD for the pulsatile flow. (a) Top view, (b) Side view

formation.

Figure 8, illustrates colour maps of WSS within the device for the pulsatile flow. In this case, the WSS is also low in the top of the chamber, even though the inflow velocity at this point is higher than in the steady case. The only region of the device which shows an acceptable WSS is in the outflow region. As mentioned before, although the WSS is low in the inflow and chamber to avoid thombus formation and deposition. The valves and diaphragm, as well as operation features of the PVAD, which determine the nature of the flow, were not considered in this simulations. Nevertheless, these first simulations show that the model was able to represent the flow with high quality of details, in which a in vitro experement is not possible.

4 DISCUSSION

In this work we have investigated the performance of the 35 cc InCor PVAD, applying steady and pulsatile flows in the inflow condition. In both cases, we observed points of stagnation flow and regions of low WSS, which are critical areas for clot formation and deposition on the segmented polyurethane, as well as the flow does not establish a good rotational "washing" pattern in the chamber. However, the diaphragm and valves were removed, as well as the operation features were not considered in this model, which are the main components of the device and determine the nature of the flow within the PVAD.

The computational model developed was able to represent properly the three-dimensional flow field within the device. Hence, it allowed us to analyze the flow within the device in a level much more refined, in which is not possible in experimental data.

In the future, we will use a preliminary model of the diaphragm and heart valves, using boundary condition. In other words, the driving force and the flow direction will be defined by the diaphragm and valves, respectively, but instead of representing these elements as flexible membranes, we will use a representation by special boundary conditions.

5 ACKNOWLEDGEMENTS

The authors would like to acknowledge the support from FAPESP Project(2012/50283-6). The first author would also like to acknowledge the financial support from CAPES.

REFERENCES

[1] Hetzer, R. and Stiller, B. Technology insight: use of ventricular assist devices in children. *Nature Clinical Practice Cardiovascular Medicine* (2006) **3**(7):377–386.

[2] Pauliks, L.B. and Ündar, A. New devices for pediatric mechanical circulatory support. *Current Opinion in Cardiology* (2008) **23**:91–96.

[3] Bluestein, D., Chandran, K.B. and Manning, K.B. Towards non-thrombogenic performance of blood recirculating devices. *Annuals of Biomedical Engineering* (2010) **38**(3):1236–1256.

[4] Ferrara, E., Muramatsu, M., Christensen, K.T. and Cestari, I.A. Particle-image velocimetry study of a pediatric ventricular assist device. *Journal of Biomechanical Engineering* (2010) **132**:071004-1.

[5] Ishino, K., Loebe, M., Uhlemann, F., Weng, Y., Hennig, E. and Hetzer, R. Circulatory support with paracorporeal pneumatic ventricular assist device (vad) in infants and childre. *European Journal of Cardio-Thoracic Surgey* (1997) **11**:965–972.

[6] Sutera, S.P. and Mehrjandi, M.H. Deformation and fragmentation of human red blood cells in turbulent shear flow. *Biophysical Journal* (1975) **15**:1–10.

[7] David, T., Thomas, S. and Walker, P.G. Platelet decomposition in stagnation point flow: an analytical and computation simulation. *Medical Engineering & Physics* (2001) **23**:229–312.

[8] Karniadakis, G.E. and Sherwin, S.J. *Spectral/hp Element Methods for Computational Fluid Dynamics*. 2nd edn. Oxford University Press, (2005).

[9] Vicent, P.E., Plata, A.M., Hunt, A.A.E., Weinberg, P.D. and Sherwin, S.J. Blood flow in the rabbit aortic arch and descending thoracic aorta. *Journal of the Royal Society Interface* (2011) **8**:1708–1719.

[10] Peiffer, V., Rowland, E.M., Cremers, S.G., Weinberg, P.D. and Sherwin, S.J. Effect of aortic taper on patterns of blood flow and wall shear stress in rabbits: Association with age. *Atherosclerosis* (2012) **223:**114–121.

[11] Volino, P. and Magnenat-Thalman, N. The SPHERIGON: a simple polygon patch for smoothing quickly your polygonal meshes. In *Proc. of Computer Animation* (1998) 72–78, 8–10 June, Philadelphia, PA, USA. Los Alamitos, CA: IEEE Computer Society

[12] A. M. Plata. A Computational Study of Blood Flow and Vascular Nitric Oxide. *A computational study of blood flow and vascular nitric oxide transport*. PhD thesis, Imperial College London, 2010.

[13] Hubbell, J.T. and McIntire, L.M. Visualization and analysis of mural thrombogenesis on collagen, polyurethane and nylon. *Biomaterials* (1986) **7**:114–121.

[14] Stuart, J. and Kenny, M.W. Blood rheology. *Journal of Clinical Pathology* (1980) **33**: 114–121.